Hybrid Materials

Deutsche Ausgabe: DOI: 10.1002/ange.201601341
Internationale Ausgabe: DOI: 10.1002/anie.201601341

Grafting Poly(3-hexylthiophene) from Silicon Nanocrystal Surfaces: Synthesis and Properties of a Functional Hybrid Material with Direct Interfacial Contact

*Muhammad Amirul Islam, Tapas K. Purkait, Md Hosnay Mobarok, Ignaz M. D. Hoehlein, Regina Sinelnikov, Muhammad Iqbal, Doron Azulay, Isaac Balberg, Oded Millo, Bernhard Rieger, and Jonathan G. C. Veinot**

Abstract: *Hybrid functional materials (HFMs) comprised of semiconductor nanoparticles and conjugated polymers offer the potential of synergetic photophysical properties. We have developed HFMs based upon silicon nanocrystals (SiNCs) and the conductive polymer poly(3-hexylthiophene) (SiNC@P3HT) by applying surface-initiated Kumada catalyst transfer polycondensation (SI-KCTP). One unique characteristic of the developed SiNC@P3HT is the formation of a direct covalent bonding between SiNCs and P3HT. The presented method for obtaining direct interfacial attachment, which is not accessible using other methods, may allow for the development of materials with efficient electronic communication at the donor–acceptor interfaces. Systematic characterization provides evidence of a core–shell structure, enhanced interfacial electron and/or energy transfer between the P3HT and SiNC components, as well as formation of a type-II heterostructure.*

The properties of semiconductor nanoparticles (or quantum dots) can be readily designed to address the needs for a multitude of applications.[1–4] This exquisite tunability is achieved by tailoring nanoparticle size, shape, and surface chemistry.[2,3,5] Similarly, the properties of π-conjugate polymers may also be tuned and complement those of quantum dots.[6–8] Hybrid functional materials (HFMs) combining nanomaterials and polymers can exhibit unique and tunable properties that may not otherwise be observed in the individual components.[7,9–11] In particular HFMs made up of compound semiconductor (for example, CdSe) nanoparticles and conjugated polymers have shown promise as functional materials in solar cells,[12,13] light-emitting diodes,[14,15] photodetectors,[16] photocatalysis,[17] and photothermal therapy.[18]

[*] M. A. Islam, Dr. T. K. Purkait, Dr. M. H. Mobarok, R. Sinelnikov, Dr. M. Iqbal, Prof. Dr. J. G. C. Veinot
Department of Chemistry, University of Alberta
11227 Saskatchewan Drive, Edmonton, Alberta, T6G 2G2 (Canada)
E-mail: jveinot@ualberta.ca
Dr. I. M. D. Hoehlein, Prof. Dr. B. Rieger
Wacker-Lehrstuhl für Makromolekulare Chemie
Technische Universität München
Lichtenbergstrasse 4, 85747 Garching (Germany)
Dr. D. Azulay, Prof. I. Balberg, Prof. O. Millo
Racah Institute of Physics, The Hebrew University of Jerusalem
Jerusalem 91904 (Israel)
Supporting information and the ORCID identification number(s) for the author(s) of this article can be found under http://dx.doi.org/10.1002/anie.201601341.

While HFMs based upon metal chalcogenide and metal oxide nanoparticles with conjugated polymers have received much attention, similar materials involving silicon nanoparticles remain relatively unexplored. Silicon is abundant, environmentally benign, and is widely used in electronic devices.[19–21] More importantly, state-of-the-art methods for preparing silicon nanocrystals (SiNCs) now afford tangible quantities of well-defined materials, the band gap of which may be tuned in the range of ca. 1.1–2.1 eV.[20,22] Furthermore, advanced procedures for tailoring NC surface functionalities now provide convenient approaches for designing their electronic[20] and optical properties.[23] Clearly, SiNCs are an attractive component on which HFMs may be formed. A few examples of physical blends made up of silicon nanoparticles with conjugated polymers have appeared.[13,24–26] However, to our knowledge, no reports of direct grafting of conjugated polymers onto or from the surfaces of well-defined SiNCs have appeared.

Herein, we report a new method that effectively interfaces conjugated polymers with SiNCs. In this study, P3HT was directly grafted from SiNC surfaces utilizing a variation of surface-initiated Kumada catalyst transfer polycondensation (SI-KCTP).[27] Subsequently, the photophysical properties of the resulting SiNC@P3HT hybrid were evaluated to ascertain the impact of directly attaching P3HT to SiNCs.

To achieve our goal of covalently interfacing SiNCs with P3HT, it was necessary to generate surface-bonded initiator sites. This was achieved by introducing an aromatic halide to the NC surface (Scheme 1). The moiety of choice for the present preparation was 2-bromo-3-hexyl-5-thienyl because it is expected to limit interfacial effects. Amongst the various strategies available for modifying SiNC surface chemistry,[10,19] reaction of hydride (that is, Si–H) surfaces with Grignard reagents was chosen because it allows for direct bonding of the thiophene ring to SiNC (Scheme 1).[28,29]

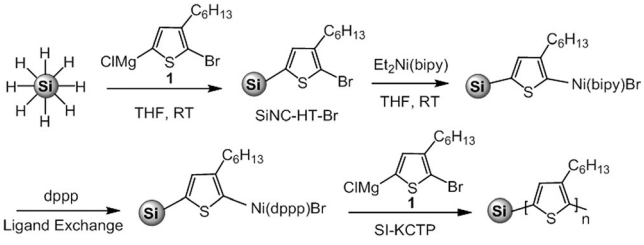

Scheme 1. The preparation of a SiNC@P3HT hybrid material.

Accordingly, hydride-terminated SiNCs (H-SiNCs) were prepared using a well-established procedure developed in our laboratories[30] and subsequently treated with 5-chloromagnesio-2-bromo-3-hexylthiophene (**1**) to obtain 2-bromo-3-hexyl-5-thienyl (-HT-Br)-terminated SiNC (SiNC-HT-Br) (Scheme 1).

Transmission electron microscopy (TEM) afforded an average diameter of 11.1 ± 1.1 nm for SiNC-HT-Br (Figure 1a). Effective introduction of the -HT-Br functionality onto the SiNC surface was evidenced by the appearance of characteristic C–H stretching (2850–2950 cm^{-1}) and C–H bending (1400–1465 cm^{-1}) in the FTIR spectrum (Figure 1b) that arise from the hexyl chain. High-resolution X-ray photoelectron spectroscopy (HR-XPS; Figure 1c–e) further supports functionalization, showing Si 2p, S 2s, and Br 3d emissions.

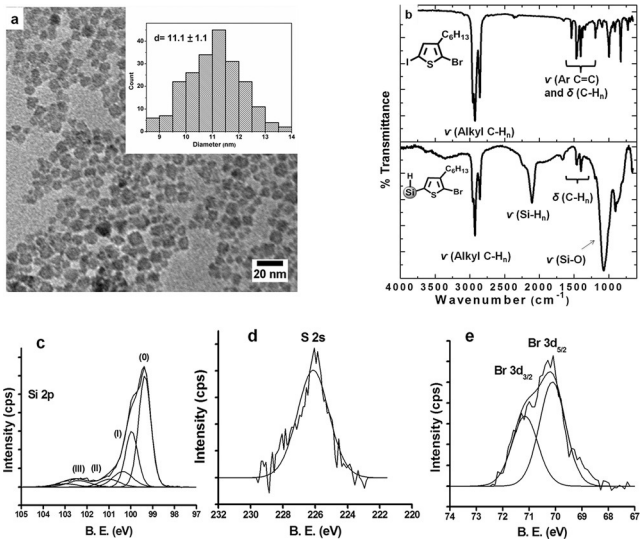

Figure 1. a) Bright-field TEM image of SiNC-HT-Br (inset: particle size distribution showing average diameter of 11.1 ± 1.1 nm). b) FTIR spectra of I-HT-Br (top) and SiNC-HT-Br (bottom). c) Si 2p, d) S 2s, and e) Br 3d regions of the high resolution XP spectra of SiNC-HT-Br.

Having introduced reactive -HT-Br moieties to the surface of SiNCs, P3HT was grafted from the particles as outlined in Scheme 1. $Et_2Ni(bipy)$ catalysts were immobilized onto the aromatic bromide termini followed by ligand exchange of bipyridine (bipy) with 1,3-Bis(diphenylphosphino)propane (dppp) to yield an orange dispersion of SiNC-HT-Ni(dppp)-Br. SI-KCTP was subsequently performed by adding monomer **1** to the SiNC-HT-Ni(dppp)-Br followed by stirring for 12 h at 25 °C under a dry nitrogen atmosphere. The resulting SiNC@P3HT hybrid was isolated and purified as described in the provided experimental procedure.

The FTIR spectrum (Figure 2a) of the SiNC@P3HT hybrid exhibits features at 3060, 2850–2950, and 1360–1600 cm^{-1} that we assign to aromatic C–H stretch, aliphatic C–H stretch, and C=C stretch/C–H bending absorptions, respectively. Figure 2b shows the Si 2p and S 2s regions of the XP spectrum of the SiNC@P3HT hybrid; consistent with

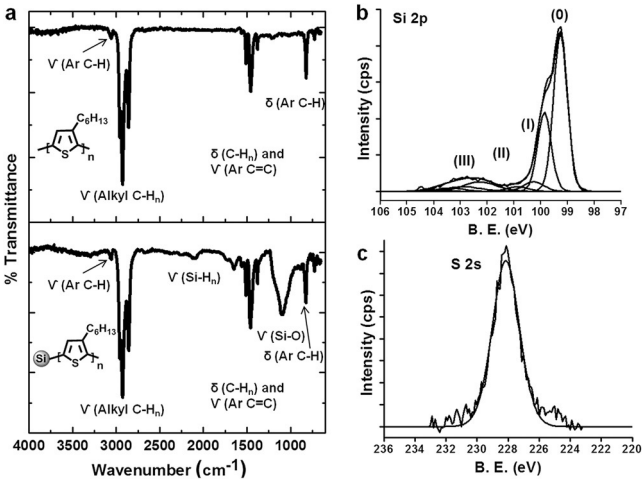

Figure 2. a) FTIR spectra of P3HT (top) and SiNC@P3HT (bottom). b) Si 2p and c) S 2s regions of the high-resolution XP spectrum of SiNC@P3HT.

surface grafting of P3HT. We note an approximate 8-fold increase in the ratio of S over Si compared to SiNC-HT-Br.

A complementary suite of electron microscopy techniques and associated spectroscopic methods provide valuable insight into the core–shell structure of the present hybrid. Bright field TEM analysis of SiNC@P3HT (Figure 3a; Supporting Information, Figure S1) shows an increase in particle diameter by about 4 nm compared to the parent SiNC-HT-Br that is attributed to the shell of P3HT.

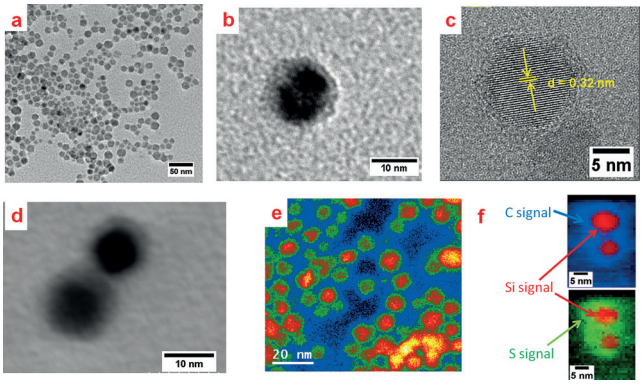

Figure 3. Electron microscopy imaging and elemental analyses of SiNC@P3HT: a) Bright-field TEM image, b) low-resolution TEM image of SiNC@P3HT core–shell, c) high-resolution TEM image of SiNC@P3HT; d) STEM bright field and e) HAADF images showing core–shell structures, f) EELS mapping of two neighboring particles.

A representative high magnification bright-field TEM image of a SiNC@P3HT particle (Figure 3b) shows expected *z*-contrast resulting from a core–shell structure. HR-TEM evaluation of SiNC@P3HT (Figure 3c) shows lattice fringes separated by 0.32 nm indicative of Si (111) lattice planes[31] confirming the crystalline Si core remained intact throughout the modification procedure. Furthermore, "hairy" features are apparent in the HR-TEM surrounding the SiNC core

consistent with a P3HT coating. Scanning transmission electron microscopy (STEM) and high annular angular dark field (HAADF) images clearly show core–shell structures (Figure 3 d,e). Electron energy loss spectroscopy (EELS) mapping of two particles (Figure 3 f) exhibits a Si rich core while the shell is rich in carbon and sulfur. Moreover, an EELS line scan spectrum (Supporting Information, Figure S2) of a representative single particle indicates the intensities of sulfur and carbon signals are substantially higher at particle edges while the composition of the core is dominated by silicon.

Thermogravimetric analysis (TGA) performed under continuous nitrogen flow was employed to estimate the amount of P3HT on the the SiNC@P3HT; it also provided an evaluation of SiNC@P3HT thermal stability. The SiNC@P3HT hybrid was stable up to 400 °C in nitrogen; a weight loss of approximately 23 % was observed between 400–600 °C (Supporting Information, Figure S3). This is the typical temperature range reported for pristine P3HT thermal decomposition.[32] Considering the 70 % weight loss for pristine P3HT after decomposition at 600 °C,[32] the 23 % weight loss for SiNC@P3HT hybrid corresponds to an estimated value of ca. 33 % P3HT in the hybrid.

To gain insight into the molecular weight and regioregularity of the grafted P3HT, the P3HT was degrafted from the SiNC surface upon etching with a 3:1:1 THF/49 % HF/water solution for 5 days; the resulting free P3HT was evaluated using mass spectrometry and ^{1}H NMR spectroscopic analysis. Matrix-assisted laser desorption ionization–time-of-flight (MALDI-TOF) mass spectrum (Supporting Information, Figure S4) reveals two overlapping patterns for the degrafted P3HT with peak separations of m/z 166 corresponding to the molecular weight of the hexylthiophene repeat unit. ^{1}H NMR reveals 100 % regioregular head-to-tail (HT) coupling of hexylthiophene repeat units at the sensivity of the NMR technique (Supporting Information, Figure S5).

After confirming successful grafting of P3HT on SiNCs the interfacial properties of the hybrid were investigated with UV/Vis absorption and photoluminescence (PL) spectroscopy. The spectra of the SiNC@P3HT hybrid were compared to those of pentyl-capped SiNC (pentyl-SiNCs), degrafted P3HT, and a physical mixture of pentyl-SiNC and P3HT (pentyl-SiNC/P3HT) (Supporting Information, Figure S6). The physical mixture was produced by combining pentyl-SiNCs obtained from borane-catalyzed hydrosilylation of pentene on hydride terminated SiNCs (see the experimental procedure and the Supporting Information, Figure S7)[33] with degrafted P3HT. Unlike the present hybrid, the P3HT is not covalently bonded to the SiNCs in the blend and the surface alkyl groups are expected to passivate the SiNC surface.[34] All solutions used for the presented spectroscopic studies were prepared using THF and the concentrations of SiNCs and/or P3HT were maintained the same (see the Supporting Information).

Qualitatively, solutions of pentyl-SiNC, P3HT, and pentyl-SiNC/P3HT appeared orange, while the solution of the SiNC@P3HT hybrid was red (Supporting Information, Figure S6a). The UV/Vis absorption spectra of THF solutions of pentyl-SiNC, P3HT, pentyl-SiNC/P3HT, and SiNC@P3HT are shown in the Supporting Information, Figure S6b. The absorption spectrum of a solution of pentyl-SiNCs is featureless, while that of P3HT exhibits a broad absorption from 300 to 550 nm ($\lambda_{max} = 450$ nm). The pentyl-SiNC/P3HT physical mixture displays a spectrum consistent with the straightforward sum of the absorption features of the SiNCs and P3HT components; this supports our proposal that negligible electronic interaction between P3HT and SiNCs surfaces exists. In contrast, the absorption spectrum obtained from the covalently bonded SiNC@P3HT hybrid shows a broad absorption ($\lambda_{max} = 450$ nm) attributed to the sum of hybrid constituents and new shoulders featured at 518, 555, and 620 nm.

Consistent with the MALDI-TOF analysis of polymer obtained from the degrafting of SiNC@P3HT, the maximum absorption at 450 nm indicates the presence of low-molecular-weight P3HT.[35] The shoulders at 518, 555, and 620 nm only appeared in the spectrum of the covalently bonded hybrid. Similar features have been attributed to efficient delocalization of electrons through conjugated backbone planarization with the additional requirement of inter-chain aggregation of P3HT on surface.[27]

Photoluminescence (PL) studies were used to evaluate the interfacial electronic communication between the P3HT and SiNCs (Supporting Information, Figure S6c). The integrated PL intensity obtained from the covalently bonded SiNC@P3HT hybrid shows an approximate 7-fold quenching of P3HT-based emission when compared to that of degrafted P3HT. In contrast, and highlighting the impact of the covalent surface linkage in the hybrid, only a 1.5-fold quenching of the P3HT-based PL was observed for the analogous physical mixture of degrafted P3HT and pentyl-SiNCs. Boon et al. have postulated that similar observations for TiO_2@P3HT hybrids resulted from conjugated surface linkages facilitating efficient charge transfer at the donor–acceptor interface.[32]

The combined energy and electron transfer efficiency may be determined for the present SiNC@P3HT hybrid using Equation (1):[36]

$$\Phi_{EET} = 1 - \frac{A_{P3HT}(\lambda_{exc})}{A_{Hybrid}(\lambda_{exc}) - A_{NC}(\lambda_{exc})} \bullet \frac{I_{Hybrid}}{I_{P3HT}} \quad (1)$$

where Φ_{EET} is the combined efficiency of electron and energy transfer, $A_{P3HT}(\lambda_{exc})$ is the absorption of degrafted P3HT at the excitation wavelength λ_{exc}, and $A_{Hybrid}(\lambda_{exc}) - A_{NC}(\lambda_{exc})$ is the absorption of P3HT in the hybrid; I_{Hybrid} and I_{P3HT} are integrated PL intensity of P3HT with and without SiNCs, respectively. From these analyses, Φ_{EET} was found to be 83 % for the SiNC@P3HT hybrid and 24 % for pentyl-SiNC/P3HT physical mixture (that is, blend).

To gain further insight into the electronic properties of the SiNC@P3HT hybrids, we performed scanning tunneling microscopy and spectroscopy (STM and STS) measurements. Here, we position the STM tip over a single particle and acquire tunneling $dI/dV - V$ spectra, which are proportional to the local density of states (DOS; details are given in the Supporting Information). The band-gap values extracted from these spectra (Figure 4) are about 1.4 eV, which is somewhat larger than the gap of bulk Si. This apparent band-gap widening is due to a combination of the (rather weak)

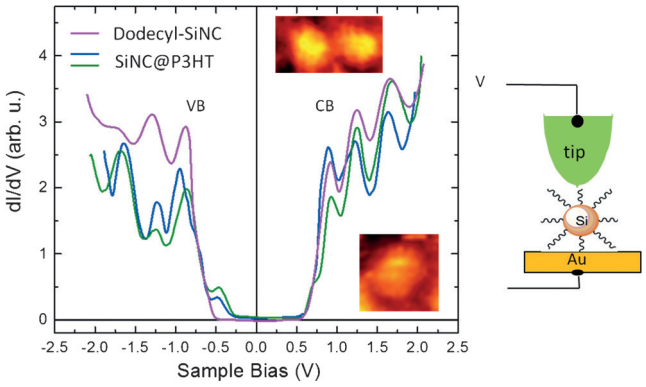

Figure 4. Tunneling d*I*/d*V*–*V* spectra measured at room temperature on SiNC@P3HT (green and blue curves), showing pronounced in-gap structure near the valance-band (VB) edge, which is absent in the spectrum acquired form a SiNC functionalized with dodecene (magenta curve). These states are attributed to the HOMO level of P3HT. The lower inset shows a topographic image of the NC on which the blue spectrum was measured, while the magenta curve was measured on the right NC shown in the upper topographic image. The double-barrier tunnel junction measurement configuration is shown to the right.

quantum confinement and the voltage division between the two tunnel junctions involved in the measurement (Figure 4).[37] Importantly, an in-gap spectral structure emerged in the DOS close to the valance-band (VB) edge, which is absent in spectra measured of alkyl functionalized SiNCs of the same size (11.2 ± 1.2 nm). This in-gap state can be associated with the HOMO level of P3HT, which is consistent with suggested models for Si-P3HT junctions.[38] The LUMO level should reside well within the conduction band of the SiNCs, where the DOS is relatively large, and therefore cannot be detected in our measurements.

In conclusion, a covalently bonded SiNC@P3HT hybrid was successfully prepared by applying surface-initiated Kumada catalyst transfer polycondensation. The resulting hybrid exhibits physical and optical properties that differ substantially from those of a physical mixture of SiNCs and P3HT. The direct linkage of SiNC to P3HT through a conjugated covalent bond gives rise to new features in the absorption and tunneling spectra, along with enhanced interfacial electronic communication.

Acknowledgements

The U of A team recognizes the Natural Science and Engineering Research Council of Canada (NSERC) Discovery Grant program for continued generous financial support. The U of A and TUM teams also recognize financial contributions from the ATUMS training program supported by NSERC CREATE and DFG IRTG (IRTG 2022) programs. MAI thanks Alberta Innovates-Technology Futures (AITF) for a Graduate Student Scholarship. Dr. J. Washington and A. K. Swarnakar are acknowledged for editing and experimental assistance. Thanks are conveyed to all Veinot Team members for thoughtful discussions.

Keywords: hybrid materials · interfaces · nanocrystals · poly(3-hexylthiophene) · silicon

How to cite: *Angew. Chem. Int. Ed.* **2016**, *55*, 7393–7397
Angew. Chem. **2016**, *128*, 7519–7523

[1] D. A. Hines, P. V. Kamat, *ACS Appl. Mater. Interfaces* **2014**, *6*, 3041–3057.
[2] R. Freeman, J. Girsh, I. Willner, *ACS Appl. Mater. Interfaces* **2013**, *5*, 2815–2834.
[3] J. Y. Kim, O. Voznyy, D. Zhitomirsky, E. H. Sargent, *Adv. Mater.* **2013**, *25*, 4986–5010.
[4] M. A. Islam, T. K. Purkait, J. G. C. Veinot, *J. Am. Chem. Soc.* **2014**, *136*, 15130–15133.
[5] H. Choi, Y.-S. Chen, K. G. Stamplecoskie, P. V. Kamat, *J. Phys. Chem. Lett.* **2015**, *6*, 217–223.
[6] J. Liu, T. Tanaka, K. Sivula, A. P. Alivisatos, J. M. J. Frechet, *J. Am. Chem. Soc.* **2004**, *126*, 6550–6551.
[7] Y. Park, R. C. Advincula, *Chem. Mater.* **2011**, *23*, 4273–4294.
[8] M. Wright, A. Uddin, *Sol. Energy Mater. Sol. Cells* **2012**, *107*, 87–111.
[9] A. A. Lutich, A. Poschl, G. Jiang, F. D. Stefani, A. S. Susha, A. L. Rogach, J. Feldmann, *Appl. Phys. Lett.* **2010**, *96*, 083109.
[10] M. Dasog, J. Kehrle, B. Rieger, J. G. C. Veinot, *Angew. Chem. Int. Ed.* **2016**, *55*, 2322–2339; *Angew. Chem.* **2016**, *128*, 2366–2384.
[11] J. Kehrle, I. M. D. Höhlein, Z. Yang, A. Jochem, T. Helbich, T. Kraus, J. G. C. Veinot, B. Rieger, *Angew. Chem. Int. Ed.* **2014**, *53*, 12494–12497; *Angew. Chem.* **2014**, *126*, 12702–12705.
[12] W. U. Huynh, J. J. Dittmer, A. P. Alivisatos, *Science* **2002**, *295*, 2425–2427.
[13] C.-Y. Liu, Z. C. Holman, U. R. Kortshagen, *Nano Lett.* **2009**, *9*, 449–452.
[14] N. Tessler, V. Medvedev, M. Kazes, S. Kan, U. Banin, *Science* **2002**, *295*, 1506–1508.
[15] B. O. Dabbousi, M. G. Bawendi, O. Onitsuka, M. F. Rubner, *Appl. Phys. Lett.* **1995**, *66*, 1316–1318.
[16] F. Guo, B. Yang, Y. Yuan, Z. Xiao, Q. Dong, Y. Bi, J. Huang, *Nat. Nanotechnol.* **2012**, *7*, 798–802.
[17] G. Liao, S. Chen, X. Quan, H. Chen, Y. Zhang, *Environ. Sci. Technol.* **2010**, *44*, 3481–3485.
[18] C. M. Hessel, V. P. Pattani, M. Rasch, M. G. Panthani, B. Koo, J. W. Tunnell, B. A. Korgel, *Nano Lett.* **2011**, *11*, 2560–2566.
[19] X. Cheng, S. B. Lowe, P. J. Reecec, J. J. Gooding, *Chem. Soc. Rev.* **2014**, *43*, 2680–2700.
[20] O. Wolf, M. Dasog, Z. Yang, I. Balberg, J. G. C. Veinot, O. Millo, *Nano Lett.* **2013**, *13*, 2516–2521.
[21] K. Sun, S. Shen, Y. Liang, P. E. Burrows, S. S. Mao, D. Wang, *Chem. Rev.* **2014**, *114*, 8662–8719.
[22] Z. Kang, C. H. A. Tsang, N.-B. Wong, Z. Zhang, S.-T. Lee, *J. Am. Chem. Soc.* **2007**, *129*, 12090–12091.
[23] T. Zhou, R. T. Anderson, H. Li, J. Bell, Y. Yang, B. P. Gorman, S. Pylypenko, M. T. Lusk, A. Sellinger, *Nano Lett.* **2015**, *15*, 3657–3663.
[24] S. Niesar, W. Fabian, N. Petermann, D. Herrmann, E. Riedle, H. Wiggers, M. S. Brandt, M. Stutzmann, *Green* **2011**, *1*, 339–350.
[25] C.-Y. Liu, Z. C. Holman, U. R. Kortshagen, *Adv. Funct. Mater.* **2010**, *20*, 2157–2164.
[26] S. Kim, K. Jeon, J. C. Lee, M. T. Swihart, M. Yang, *Appl. Phys. Express* **2012**, *5*, 022302.
[27] V. Senkovskyy, R. Tkachov, T. Beryozkina, H. Komber, U. Oertel, M. Horecha, V. Bocharova, M. Stamm, S. A. Gevorgyan, F. C. Krebs, A. Kiriy, *J. Am. Chem. Soc.* **2009**, *131*, 16445–16453.
[28] N. Y. Kim, P. E. Laibinis, *J. Am. Chem. Soc.* **1998**, *120*, 4516–4517.
[29] I. M. D. Höhlein, A. Angı, R. Sinelnikov, J. G. C. Veinot, B. Rieger, *Chem. Eur. J.* **2015**, *21*, 2755–2758.

[30] C. M. Hessel, E. J. Henderson, J. G. C. Veinot, *Chem. Mater.* **2006**, *18*, 6139 – 6146.
[31] Z. Kang, C. H. A. Tsang, Z. Zhang, M. Zhang, N.-B. Wong, J. A. Zapien, Y. Shan, S.-T. Lee, *J. Am. Chem. Soc.* **2007**, *129*, 5326 – 5327.
[32] F. Boon, D. Moerman, D. Laurencin, S. Richeter, Y. Guari, A. Mehdi, P. Dubois, R. Lazzaroni, S. Clement, *Langmuir* **2014**, *30*, 11340 – 11347.
[33] T. K. Purkait, M. Iqbal, M. H. Wahl, K. Gottschling, C. M. Gonzalez, M. A. Islam, J. G. C. Veinot, *J. Am. Chem. Soc.* **2014**, *136*, 17914 – 17917.
[34] D. J. Milliron, A. P. Alivisatos, C. Pitois, C. Edder, J. M. J. Frechet, *Adv. Mater.* **2003**, *15*, 58 – 61.
[35] S. K. Sontag, G. R. Sheppard, N. M. Usselman, N. Marshall, J. Locklin, *Langmuir* **2011**, *27*, 12033 – 12041.
[36] A. A. Lutich, G. Jiang, A. S. Susha, A. L. Rogach, F. D. Stefani, J. Feldmann, *Nano Lett.* **2009**, *9*, 2636 – 2640.
[37] U. Banin, O. Millo, *Annu. Rev. Phys. Chem.* **2003**, *54*, 465 – 492.
[38] J. C. Nolasco, R. Cabré, J. Ferré-Borrull, L. F. Marsal, M. Estrada, J. Pallarès, *J. Appl. Phys.* **2010**, *107*, 044505.

Received: February 5, 2016
Published online: May 4, 2016

